https://doi.org/10.20965/ijat.2021.p0503

Technical Paper:

Study on the SUAM Double Magnet System for Polishing

Tatsuya Nakasaki†, Yushi Kinoshita, Panart Khajornrungruang, Edmund Soji Otabe, and Keisuke Suzuki

Kyushu Institute of Technology
680-4 Kawazu, Iizuka, Fukuoka 820-8502, Japan
†Corresponding author, E-mail: nakasaki.tatsuya257@mail.kyutech.jp
[Received January 18, 2021; accepted May 24, 2021]

Superconductive assisted machining (SUAM) is a novel machining method that eliminates tool interference via magnetic levitation tools. In our study, we developed a double magnet system (DMS) to increase the maximum power of the holding force and stabilize the magnetic rotation during polishing via the higher magnetic flux compared to a single magnet system (SMS). The maximum magnetic flux density of the DMS was approximately 100 mT higher than that of the SMS. In these cases, the entire holding force increases as the distance between the superconducting bulk and lower magnet decreases. The attractive forces are maximum around a displacement of 6 mm, although the repulsive and restoring forces increase spontaneously. The polishing performances of the DMS on the SUS304 and A1100P plates were evaluated using water-based diamond slurries, for equal levitation amounts. The amount removed by the DMS increased for the A1100P and SUS304 substrates compared to that by the SMS. In this case, we observe that the deviation of the polishing area on the DMS decreases compared to that of the SMS, reflecting a more stable rotation and movement due to the higher holding force.

Keywords: superconductor, double magnet system, magnetic levitation tool, grinding/polishing

1. Introduction

Recently, mass-production machining technology with high precision/speed processing has been developed for multi-axis machining centers [1–4]. As the complexity of machined shapes evolves, advanced programs are needed to avoid tool interference and fabricate the desired shape. However, the problems of tool interference become serious as the machining complexity increases. Superconductive assisted machining (SUAM) – which uses the flux-pinning phenomenon [5–7] on superconductive bulk – has been proposed to reduce tool interference and levitate magnet-embedded tools, as shown in **Fig. 1**. In this case, the magnetic levitation tool moves along the inner walls of the hollow object via the holding force,

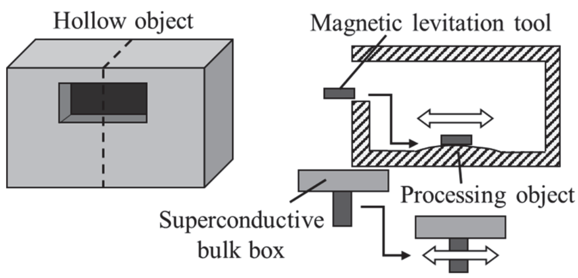

Fig. 1. Example of machining a hollow object using the magnetic levitation tools.

moving in parallel in the XY stage and inclination in the θ stage. It is also possible to switch the machining position and force by adjusting the Z-stage displacement. This flux-pinning phenomenon occurs in type-II superconductors. This phenomenon can be explained by the fact that the external magnetic field penetrates the defects into the superconductive bulk and is pinned at the inner normally conductive parts at the defects. This study used rare-earth-based superconductive materials that result in a flux-pinning effect via a liquid nitrogen cooling process [8–13]. Some superconductive characteristics, such as pinning effects and diamagnetic and zero electrical resistance, have been applied in superconductive bearings [14, 15], conveyors [16, 17], and superconductive magnets [18]. In addition to these technologies, we focus on SUAM because the levitation tools in the air can be processed as long and bent tubes and ribs inside the deep hole via conventional processing methods. Levitation tools using Nd permanent magnets will be trapped in the air and move while being rotated via a motor equipped with an XYZ stage attached to the superconductive bulk and container. In this case, this technique does not restrict tool interference because the movement of the levitation tool can be controlled by superconducting bulk movement. Therefore, by setting the XYZ and inclined-stage motion, it is possible to selectively machine the necessary parts of the inner surface of the hollow objects, or even more complicated shapes. In a previous study, we suggested using a DMS to increase the magnetic flux on the pinning effect via upper and lower magnets to increase the levitation amount and attractive force [7].

© Fuji Technology Press Ltd. Creative Commons CC BY-ND: This is an Open Access article distributed under the terms of the Creative Commons Attribution-NoDerivatives 4.0 International License (http://creativecommons.org/licenses/by-nd/4.0/).

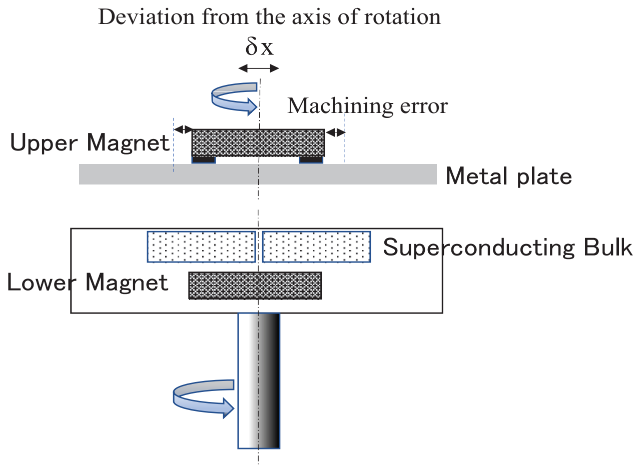

Fig. 2. Schematic diagram of the DMS. This figure indicates some issues of SUAM.

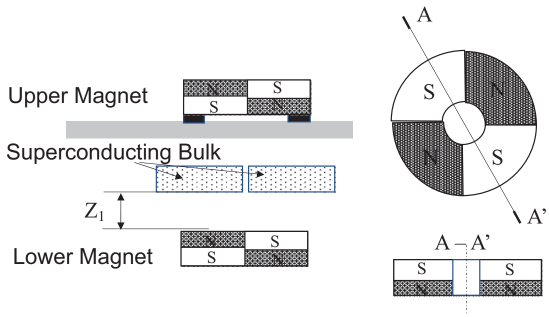

Fig. 3. Layout of the upper and lower magnets against superconducting bulks.

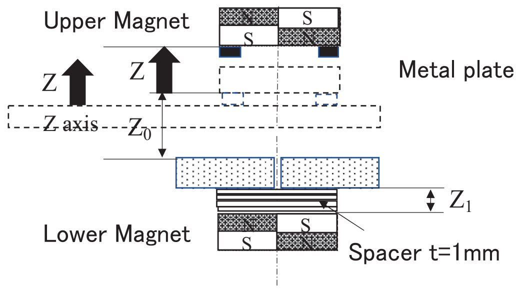

Fig. 4. Distances Z_0, Z, and Z_1 on the DMS.

In this study, the polishing efficiency of the DMS on the metal substrates was higher than that of the SMS because a higher polishing pressure can be generated by the attractive force. Hence, we need to evaluate not only the attractive force but also the repulsive force, resorting force, and driving force to consider the polishing parameters under several DMS conditions. In the present study, we evaluated the magnetic flux on the DMS and the holding force at several distances between the upper/lower magnets from the superconducting bulks. We then compared the polishing areas of the SMS and DMS using aluminum (A1100P) and stainless steel (SUS304) plates to estimate the stability of the tool rotation and movements during polishing.

2. Concept of the DMS

A schematic diagram of the DMS is shown in **Fig. 2**. This double-magnet system has two permanent magnets placed at the upper and lower sides of the semiconducting bulk. An upper magnet was used as the magnetic levitation tool. The levitating amount of the magnet was determined using a jig during the cooling process. After the jig was removed, the upper magnet was fixed in the air at the initial position. When the SUS substrate moves in the upper direction, an attractive force is generated because the upper magnet acts to return to its initial position. In this case, the deviation of the axis by rotation is generated during rotation because the upper tool is not fixed by a rigid spindle but only by the holding force. If the axis of rotation of the magnet deviates from the center at the fixed process by the jig, it will cause run-out tolerance. In the case of a weak holding force, the deviation amount might be increased by the centrifugal force. In addition, the tool position might also be shifted by the friction generated between the tools and SUS or aluminum plates. Therefore, we need to optimize the distance between the upper and lower magnets and the superconducting bulk to realize stable and high-efficiency polishing via the DMS.

Figure 3 shows the layout of the upper and lower magnets against the superconducting bulks. There are four superconductive bulks placed in a container; each is 35 mm × 35 mm × 10 mm (length × width × height). These superconducting bulks are placed evenly inside the container the same as previous report [6]. These bulks are made of a rare-earth-based type-II superconductor ($GdBa_2Cu_3O_x$) that transitions to a superconducting state under liquid nitrogen temperatures. The N pole and S pole face each other between the upper and lower magnets. In this experiment, the magnetic flux density and several holding forces were measured at various Z_1 positions.

Figure 4 illustrates the distances Z_0, Z, and Z_1 in the DMS. Z is determined by the jig to fix the initial position in the magnetic field during the cooling process. After the upper magnet was trapped in the air, the jig was removed. Z can be adjusted by the movement of the SUS plate attached to the Z-axis stage. Z_1 is set by a 1 mm thick spacer inserted between the superconducting bulks and lower magnet. In our experimental system, Z_1 varied from 4 to 20 mm.

3. Performance of the DMS System

3.1. Evaluation of Magnetic Flux Density

We have developed a DMS device based on JMAG simulation [19]. This calculation predicts that the magnetic flux density and holding force of the upper magnet increase as the distance Z_1 decreases. Therefore, we evalu-

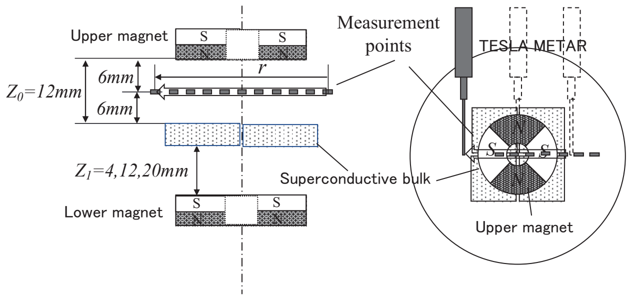

Fig. 5. Magnetic flux density measurement system.

Table 1. Measurement conditions for magnetic flux density.

Initial position height of upper magnet Z_0	12 mm
Initial position height of lower magnet Z_1	4, 12, 20 mm
Measurement point r	0, 10, 20, 30, 40, 50, 60, 70, 80, 90, 100 mm
Superconductive bulk	Material: $GdBa_2Cu_3O_x$ Made: Nippon Steel Corporation Size: 35 × 35 × 10 mm Number: 4
Magnetic levitation tool and lower magnet	Material: Neodymium Size: ϕ59-ϕ19-10 Magnetic flux density: 0.4 T Pole: 4 poles on one side
Measurement tool	TESLA METER Made: Kanetec Co., Ltd. Model number: TM-801

ated the magnet flux and holding force at various Z_1 positions.

Figure 5 shows a conceptional diagram to measure the magnetic flux density. Measurement positions are set by the 6 mm distance from the top face of the superconducting bulk to adjust the same distance between the lower face of the upper magnet and the sensor. Measurement points – denoted in the side view as r – were set at 10 mm intervals from 0 mm (the origin) to 100 mm, along the radial direction. The magnet flux densities were measured at these points, in two directions (across the N and S pole regions), as shown in the top view.

Table 1 lists the measurement conditions for the magnetic flux density. The permanent Nd magnet in this study comprised four poles on each side. In the DMS device using two Nd permanent magnets in this experiment, Z_0 of the upper magnet displacement was fixed at 12 mm and the lower magnet distance, Z_1, was adjusted to 4 mm, 12 mm, and 20 mm. The magnetic flux density was measured using a TESLA METER (KANETEC, TM-801). In this measurement, the sensor position is set to the same distance of the upper magnet and superconducting bulks at 6 mm, using a jig for measurement.

3.2. Magnetic Flux Density on the DMS

Figure 6 shows the magnetic flux densities on the DMS and SMS across (a) the N pole region and (b) the S pole region. The distances of Z_1 in the DMS were 4 mm, 12 mm, and 20 mm. The maximum absolute values of the magnetic flux density were almost the same for the N pole and S pole measurements. The center of the donut shape of the Nd permanent magnets was located at 45 mm. In these cases, the peaks of the magnet flux density were at distances of approximately 30 mm and 70 mm around the central areas of each pole. The magnetic flux densities of the DMS were approximately 100 mT higher than that of the SMS. The magnetic flux density increases with decreasing magnet distance. In this experiment, the highest magnetic flux densities of 433.7 mT and 383.0 mT were obtained for the N and S poles, respectively, for $Z_1 = 4$ mm.

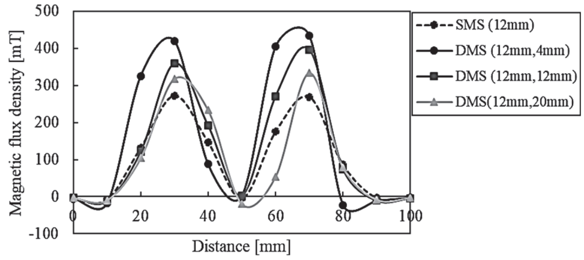

(a) N pole

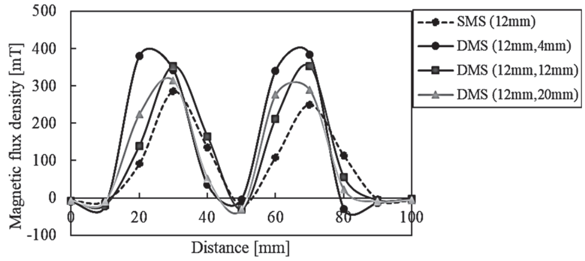

(b) S pole

Fig. 6. Magnetic flux density of the SMS and the DMS at various Z_1.

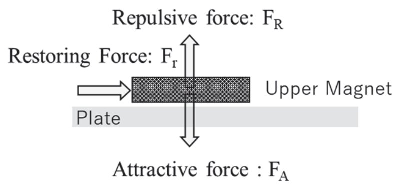

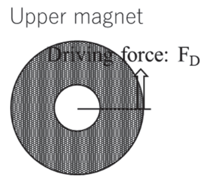

(a) Top view (b) Side view

Fig. 7. Concept of holding forces.

3.3. Measurements of Holding Force

The holding forces were measured using three load cells. **Fig. 7** shows the concept of the holding force as an attractive force, repulsive force, restoring force, and driving force.

The magnet was initially fixed in the air by the pinning effect of the superconducting bulk during the field cooling process [20]. In our study, the holding forces were measured along the vertical, horizontal, and rotational axes. In this experiment, the holding forces at the DMS were measured at different Z_1 positions of the lower magnet. The

Table 2. Measurement conditions for holding forces.

Initial position height of upper magnet Z_0	12 mm
Initial position height of lower magnet Z_1	4, 12, 20 mm
Superconductive bulk	Material: $GdBa_2Cu_3O_x$ Made: Nippon Steel Corporation Size: 35 × 35 × 10 mm Number: 4
Magnetic levitation tool and lower magnet	Material: Neodymium Size: ϕ59-ϕ19-10 Magnetic flux density: 0.4 T Pole: 4 poles on one side
Measurement tool	Load cell Made: Kyowa Electronic Instruments Co., Ltd. Model number: LMA-A-50N
	Instrumentation conditioner Made: Kyowa Electronic Instruments Co., Ltd. Model number: WGA-650B

measurement conditions for the holding force are listed in **Table 2**.

Figure 8 shows the measurement method on each force as (a) an attractive force, (b) a repulsive force, (c) a restoring force, and (d) a driving force. First, the upper magnet was trapped at the initial position Z_0 by the pinning effect. Subsequently, external forces were applied to the upper magnet. Thus, the upper magnet was located at a point where the external force and holding forces were balanced; the holding forces were measured by a load cell (Kyowa Electronic, LMA-A-50N) inside a special jig.

The attractive force is shown in **Fig. 8(a)**. The attractive force F_A at the magnetic levitation tool was generated in the downward direction when the magnetic levitation tool was displaced in the upward Z direction. In this measurement system, three load cells were mounted on the SUS plate of the special measurement jig. F_A is the sum of f_1, f_2, and f_3 from each load cell.

Figure 8(b) shows the repulsive forces. The repulsive forces were generated in the upward direction when displaced in the downward Z direction to become closer to the superconductive bulk. The repulsive force was also measured by three load cells, similar to the measurement of the attractive force.

The restoring force is shown in **Fig. 8(c)**. The restoring force F_r was generated in the horizontal direction when the tool was displaced horizontally by an external force. The restoring force was measured by the load cell at a single point.

The driving force is shown in **Fig. 8(d)**. The driving force F_D is generated along the rotational direction when the tool displaces θ by an external force. The displacement angle was adjusted in 5° increments by the controller in this device. The force was measured using a load cell inside a special jig. The measurement position of the load cell is a single point in this measurement.

In these measurements, the holding forces were measured at three Z_1 values of 4 mm, 12 mm, and 20 mm while Z_0 was fixed at 12 mm.

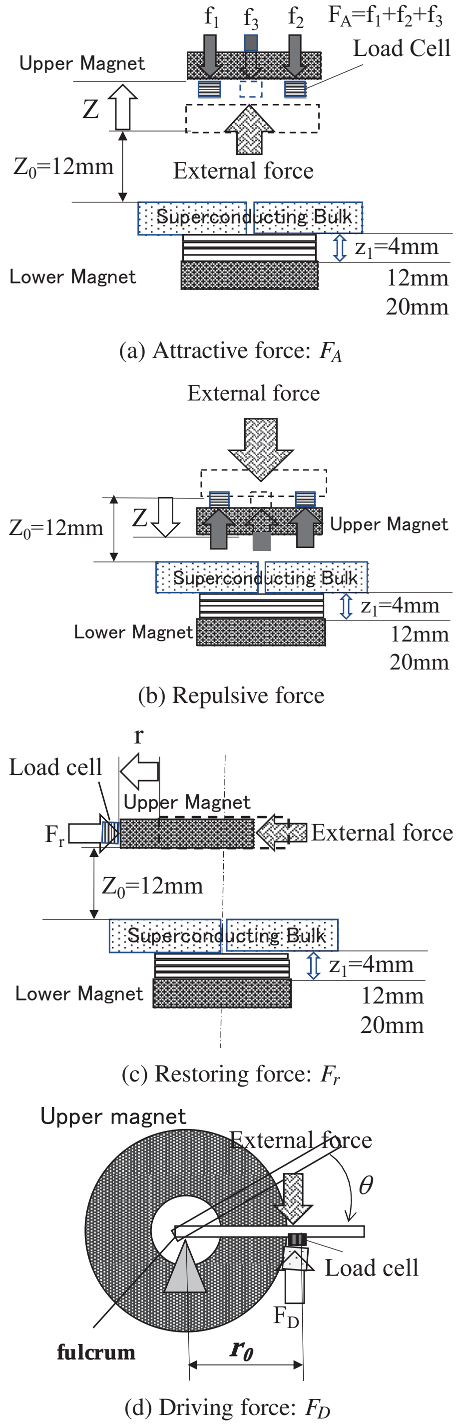

Fig. 8. Method for measuring the holding forces in the DMS.

3.4. Measurement of the Holding Forces

Figure 9 shows the holding forces for the DMS and SMS.

The attractive force results are shown in **Fig. 9(a)**. The attractive force of the DMS is higher than that of the SMS under all conditions. For the DMS, the peak attractive force increases as Z_1 decreases. When Z_1 is 4 mm, the peak attractive force is 12.96 N while the maximum value of the SMS is 5.61 N. Under all conditions, the attractive forces reached a maximum value around a displacement

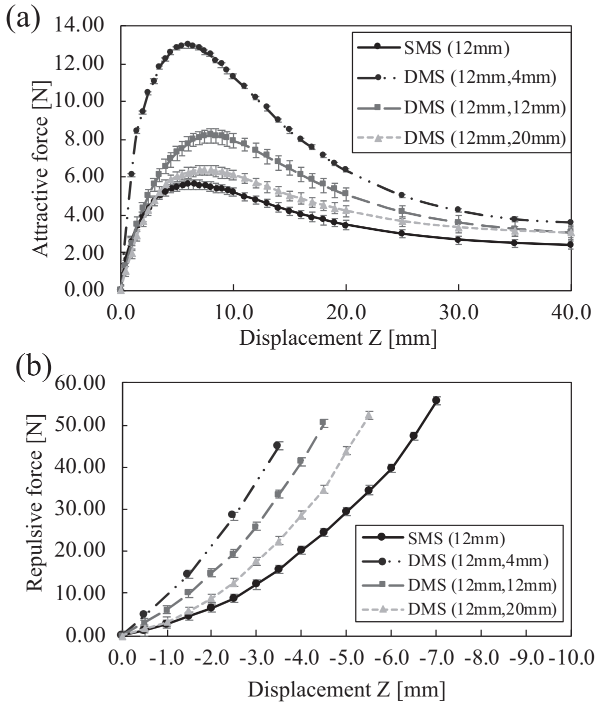

Fig. 9. Displacement Z vs. (a) attractive force and (b) repulsive force.

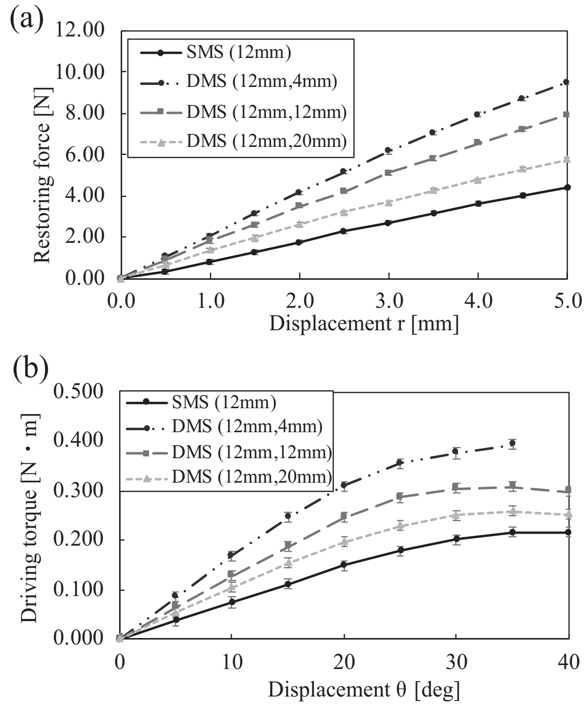

Fig. 10. Displacement r and θ vs. (a) restoring force and (b) driving torque.

of $Z = 6$ mm. The forces decrease until approximately 30 mm and converge to a constant value above 30 mm. This tendency of the attractive force curve is consistent with the JMAG analysis results, suggesting a pinning effect of the DMS. At a region beyond the maximum value of the attractive force, the magnetic flux density decreases as Z increases. The net flux density of the DMS is determined by the distance $Z_0 + Z_1 + Z$ between the upper and lower magnets, although the magnet flux density of the SMS is determined by $Z_0 + Z$. In this case, the upper magnet – which is the levitation tool – is attracted to the lower magnet, as well as by the pinning effect of the superconducting bulk. Therefore, the attractive force at $Z_1 = 4$ mm for the lower magnet increases more than at 12 mm and 20 mm. In the region over 30 mm, the variation in the attractive force becomes small. In these cases, the attractive force of the DMS is slightly higher than that of the SMS because the attractive force of the DMS is generated by the weak magnet flux between the upper and lower magnets, in addition to the weight of the upper magnet.

The repulsive force is shown in **Fig. 9(b)**. The repulsive force of the DMS significantly increases than that of the SMS. In these cases, the repulsive forces increased as the displacement Z increased. In the case of DMS, the maximum value of the repulsive force is approximately 50 N at 3.5 mm, although that of the SMS is approximately 12 N. The large change in repulsive force with respect to the displacement is caused by the magnet flux distribution between the magnets. The magnetic flux density captured by the pinning effect inside the superconducting bulk drastically increases with the lower and upper magnets because the opposite poles of both magnets are parallel to our experimental device. The polishing force using the repulsive force increases as the distance between the lower magnet and superconducting bulk decreases.

Figure 10(a) shows the restoring force. The restoring force of the DMS was also higher than that of the SMS in all conditions. The restoring force needs to exceed the total polishing resistance and dynamic friction generated at the interface between the polishing surface and tools, although the restoring force is not directly affected by polishing pressure. In this case, the polishing position by the magnetic levitation tool is controlled by the movement of the superconducting bulk box using the XY stage. Therefore, the DMS, which generates a higher restoring force, can stabilize the tool movement. The DMS can be applied to several polishing/grinding processes that generate high resistive forces during processing. The increase in the restoring force at the DMS is caused by the higher magnetic flux density at each pole between the magnetic levitation tool and the lower magnet.

Figure 10(b) shows the driving torque, calculated using the force measured by the load cell. The driving torque of the DMS was also higher than that of the SMS under all conditions. For the 4 mm DMS condition, the slow convergence might be caused by the higher magnetic flux density. The driving force also needs to be higher than the total force of polishing resistance and dynamic friction, which is the same as the restoring force. The rotation angle of the tool during polishing is determined by the balance between the driving and resistive forces during polishing. In our experiment, as the displacement θ – equivalent to the rotational angle – increases, the driving torque increases until a displacement of $\theta = 30°$.

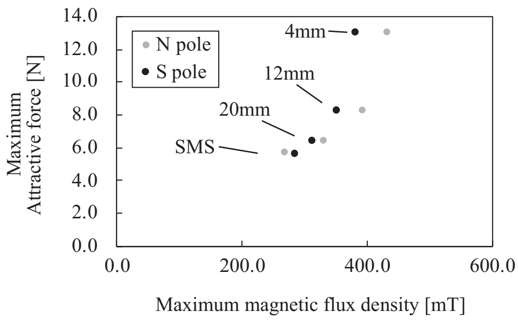

Fig. 11. Relationship between magnetic flux density and attractive force.

When the displacement θ exceeds 35°, the driving torque decreases slightly. This tendency might be caused by the magnetization position of each N and S pole during the fabrication process of the permanent magnets. Therefore, the magnetic levitating tools could not maintain rotational motion against the polishing resistance at a displacement of more than 35° because the magnetic field drastically decreases as the displacement approaches 45° around the opposite pole.

As a result, it was confirmed that the total holding force by DMS increased more than that of the SMS, resulting in improved polishing performance. In particular, stabilization of the movement and rotation of the levitation tools is expected due to the higher restoring force and driving torque during polishing.

3.5. Relationship Between Magnetic Flux Density and Attractive Force

The attractive force is an important parameter for determining the polishing pressure of SUAM. **Fig. 11** shows the relationship between the magnetic flux density and attractive force. The maximum values of the magnetic flux density and attractive force are plotted for each experimental condition in this figure. The attractive force increases as the magnetic flux density increases at the S and N pole regions of the upper magnet. In this case, the magnetic flux density of the DMS setting at $Z_1 = 4$ mm is approximately 100 mT higher than that of the SMS, resulting in an attractive force that is approximately 2 times that in the SMS. Therefore, it is confirmed that the attractive force can be strengthened by a higher magnetic flux density. Based on these experimental and JMAG calculation results, the lower magnet needs to get closer to the superconducting bulk in the DMS system to generate a high polishing pressure.

4. Polishing Performance on A1100P and SUS304

4.1. Polishing Test

The polishing performance of the SUAM was evaluated using an improved SUAM system with a double-magnet system. In this test, we compared the polishing performance of the DMS system with that of a conventional SMS system. The polishing substrates were two typical materials, i.e., A1100P with a thickness of 1 mm and SUS304 with a thickness of 0.5 mm. **Table 3** lists the polishing conditions used. The free abrasive in the water can be used in the SUAM process because the temperature around these substrates is almost room temperature. The particle diameter of the slurry was 1 μm. The diamond slurry was adjusted to a pH of 12 using a KOH powder solute. The polishing speed was set to 140 rpm and the polishing time was 10 min. **Fig. 12** shows the polishing process and the magnetic levitation tool. The

Table 3. Polishing condition.

Polishing pressure [kPa]	SMS	DMS
	55	132
Rotation speed [rpm]	140	
Polishing time	10 min	
Work (before polishing)	Aluminum: A1100P Size: 70 × 70 × 1 mm Surface roughness: Ra = 800–1000 nm Thickness of the plate = 3 mm	
	Stainless steel: SUS304 Size 75 × 75 × 0.5 mm Surface roughness: Ra = 100–200 nm Thickness of the plate = 3 mm	
Slurry	Abrasive: diamond (polycrystalline) Particle diameter: ϕ1 μm pH: 12 Made: Engis Japan Corporation Slurry flow rate: 60 mL/min	
Polishing pad	SUBA600 Size: 5.5 × 5.5 mm	

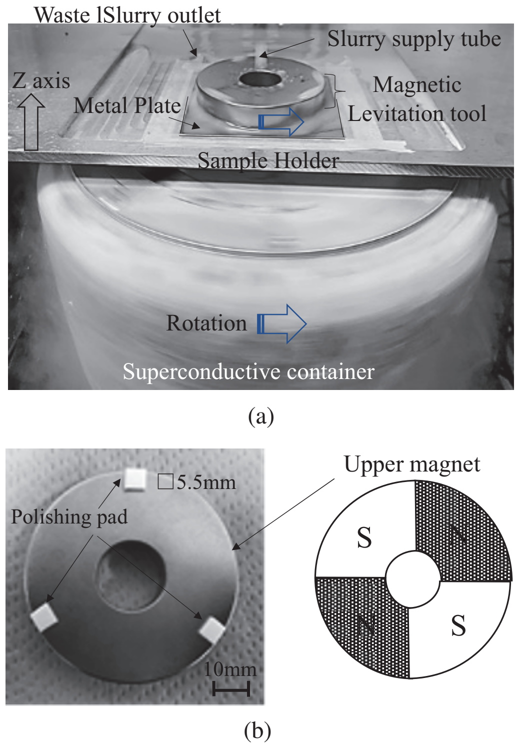

Fig. 12. Polishing system on the DMS and magnetic levitation tools.

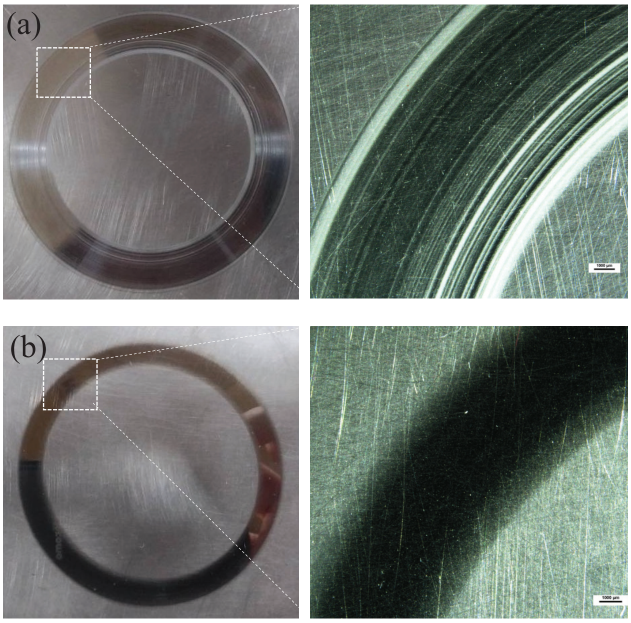

Fig. 13. Photographs the SUS304 metal plate after polishing by (a) the SMS and (b) the DMS.

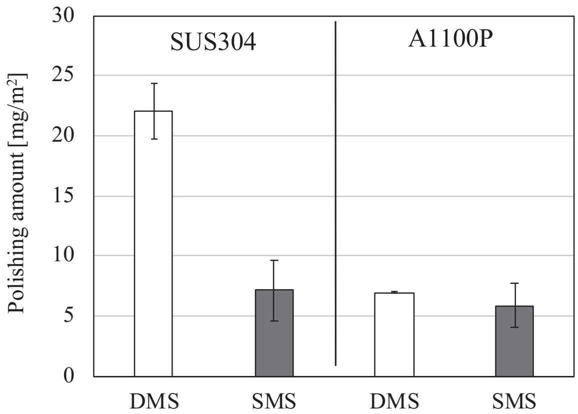

Fig. 14. Polishing amount of SUS304 and A1100P.

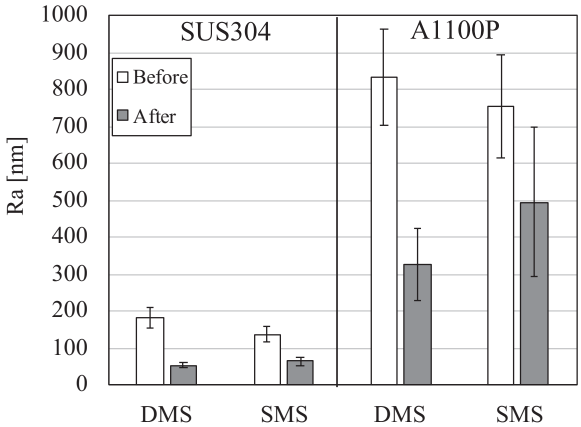

Fig. 15. Arithmetic mean roughness *Ra* of SUS304 and A1100P before and after polishing.

diamond slurry was dripped directly above the magnetic levitation tool. The slurry was collected from the port at the stage that held the workpiece. The slurry was circulated in the slurry supply system during polishing. The temperature of the diamond slurry was set at 30°C. It was constantly stirred to prevent the abrasive grains from aggregating. The initial position Z_0 of the magnetic levitation tool was set to 12 mm. Based on the measurement of the magnetic flux density and holding force, Z_1 was set to 4 mm because the attractive force was the strongest. After cooling the superconductive bulk in a magnetic field, the superconductive bulk cover was lowered by 4 mm to generate an attractive force of 5 N in the SMS and 12 N in the DMS, generating a polishing pressure. The polishing pressures were 55 kPa for the SMS and 132 kPa for the DMS, depending on the size of the pad, as shown in the right inset of **Fig. 11**. The polishing amount was measured by the gravimetric change from before- to after-polishing, via a microelectronic balance (A&D, BM-10). The surface roughness of the substrates before and after polishing was measured using a stereomicroscope (Nikon, SMZ-18) and a confocal laser microscope (KEYENCE, VR-9700).

4.2. Polishing Results

Figure 13 shows the SUS304 metal plate after polishing by the SMS and DMS. The ring shape on the substrate is the area polished by the SUBA pad. The ring width on the SMS increases by approximately 50% compared to that on the DMS. In this case, some striped lines appear in the polishing area because the rotation of the tools is not stable in the SMS. In these cases, the holding force needs to exceed the friction between the SUS substrate and tools to stabilize the tool rotation and movement.

Figure 14 shows the polishing amounts of SUS304 and A1100P substrates polished by diamond slurry. The polishing amount of the DMS is higher than that of the SMS for both substrates. For SUS304, the polishing amount of the DMS is 22.06 mg/m^2 while the polishing amount of the SMS was only 7.11 mg/m^2. The polishing amount of the DMS is approximately three times that of the SMS at the same time reflected on the higher pressure. On the other hand, the polishing amount of DMS on the A1100P substrate was slightly higher than that of SMS; this might be caused by combability between the diamond slurry and aluminum substrate because of the same polishing pressure for both substrates.

Figure 15 shows the *Ra* of the surface roughness on the SUS304 and A1100P substrates before and after polishing. The *Ra* of the surface roughness was calculated from the image data of the confocal laser microscope. In these cases, variations in *Ra* before and after polishing on each substrate were estimated to evaluate the planarization ability of the polishing at the DMS and SMS processes. In the case of the SUS304 substrate, the variation in *Ra* before and after polishing was 132 nm for the DMS. This value is higher than the 74 nm of the SMS, even at the same polishing time. Therefore, the polishing performance of the DMS exhibits not only a high removal amount but also a high planarization ability compared to the SMS, as reflected by the higher polishing pressure. For the A1100P substrate, the variation in *Ra* before and after polishing was 506 nm for the DMS. This value is also higher than 260 nm for the SMS. These improvements in surface roughness on DMS can be attributed to the higher holding force required to stabilize the movement of the magnetic levitation tools.

5. Summary

1. We propose that the DMS generates a higher holding force against the SMS. In this case, the DMS can improve polishing accuracy because the tool rotation and movement become stable at a higher holding force against SMS.
2. The magnetic flux density in the DMS increases as the initial position of the lower magnet approaches the superconductive bulk. In our experimental system, all holding forces were maximum when Z_1 was set to 4 mm.
3. The maximum magnetic flux density of the DMS at $Z_1 = 4$ mm is approximately 100 mT higher than that of the SMS. In these cases, the magnetic flux density increased as Z_1 decreased.
4. The polishing amount of DMS is higher than that of SMS on the SUS304 and A1100P substrates because of the higher holding force. In the case of SUS304, the polishing amount of the DMS is 22.06 mg/m^2, although that of SMS is 7.11 mg/m^2.
5. Regarding the surface roughness on the SUS304 and A1100P substrates before and after polishing, the variation in *Ra* before and after polishing on the SUS304 plate was 132 nm for the DMS, which is higher than that of the SMS.

Acknowledgements

This study was supported by JSPS KAKENHI (Grant Nos. 26630029 and 19H00771) and the Mitsui Foundation for the Advancement of Tool and Technology.

References:

[1] M. Sudo, “Advanced Control Technologies for 5-Axis Machining,” Int. J. Automation Technol., Vol.1, No.2, pp. 108-112, 2007.

[2] L. Silva, H. Yoshioka, H. Shinno, and J. Zhu, “Tool Orientation Angle Optimization for a Multi-Axis Robotic Milling System,” Int. J. Automation Technol., Vol.13, No.5, pp. 574-582, 2019.

[3] T. Suzuki, K. Yoshikawa, T. Hirogaki, E. Aoyama, and T. Ikegami, “Improved Method for Synchronizing Motion Accuracy of Linear and Rotary Axes Under Constant Feed Speed Vector at End Milling Point – Investigation of Motion Error Under NC-Commanded Motion –,” Int. J. Automation Technol., Vol.13, No.5, pp. 679-690, 2019.

[4] T. Saiki, M. Tsutsumi, H. Suzuki, M. Kouya, and M. Ushio, “Development of Measurement for Motion Accuracy of 5 Axis NC Machine Tool,” Int. J. Automation Technol., Vol.2, No.2, pp. 111-118, 2008.

[5] Y. Tanaka, K. Suzuki et al., “Study on polishing technology using magnetic levitation tools with superconductivity,” J. of the Japan Society for Abrasive Technology, Vol.62, No.4, 2018.

[6] H. Nakashima, K. Suzuki et al., “Study on Polishing Method using Magnetic Levitation Tool in Superconductive-Assisted Machining,” Int. J. Automation Technol., Vol.15, No.2, pp. 234-242, 2021.

[7] K. Suzuki, T. Nakasaki et al., “Study on polishing method using double magnet system by superconductive assisted machining method,” Proc. of Leading Edge Manufacturing/Materials & Processing (LEM&P2020), 8553, 2020.

[8] A. I. Larkin and Y. N. Ovchinnikov, “Pinning in Type II Superconductors,” J. of Low Temperature Physics, Vol.34, No.3-4, pp. 409-428, 1979.

[9] J. Bardeen, L. N. Cooper, and J. R. Schrieffer, “Theory of Superconductivity,” Physical Review, Vol.108, No.5, pp. 1175-1204, 1957.

[10] M. Tinkham and C. J. Lobb, “Physical Properties of the New Superconductors,” Solid State Physics, Vol.42, pp. 91-134, 1989.

[11] H. B. Radousky, “A Review of the Superconducting and Normal State Properties of Y1-xPrxBa2Cu3O7,” J. of Materials Research, Vol.7, No.7, pp. 1917-1955, 1992.

[12] M. K. Wu et al., “Superconductivity at 93 K in a New Mixed-Phase Yb-Ba-Cu-O Compound System at Ambient Pressure,” Physical Review Letters, Vol.58, No.9, pp. 908-910, 1987.

[13] D. He et al., “Spatial and temporal flux-trapping properties of bulk high temperature superconductors under static magnetization fields,” J. Supercond. Nov. Magn., Vol.28, pp. 2385-2391, 2015.

[14] J. R. Hull, “Superconducting Bearings,” Superconductor Science and Technology, Vol.13, No.2, pp. R1-R15, 2000.

[15] Y. Arai, H. Seino, and K. Nagashima, “Levitation Properties of Superconducting Magnetic Bearings using Superconducting Coils and Bulk Superconductors,” Superconductor Science and Technology, Vol.23, No.11, 115011, 2010.

[16] J. Wang et al., “The First Man-Loading High Temperature Superconducting Maglev Test Vehicle in the World,” Physica C: Superconductivity and its Applications, Vol.378-381, Part 1, pp. 809-814, 2002.

[17] L. Schultz et al., “Superconductively Levitated Transport System-the SupraTrans Project,” IEEE Trans. on Applied Superconductivity, Vol.15, No.2, pp. 2301-2305, 2005.

[18] L. Rossi, “The LHC superconducting magnets,” Proc. of the 2003 Particle Accelerator Conf., Portland, OR, Vol.1, pp. 141-145, doi: 10.1109/PAC.2003.1288863, 2003.

[19] Y. Hiramatsu et al., “Evaluation of Magnetic Cutting and Polishing with Superconducting Bulks,” J. of Physics: Conf. Series, Vol.871, 012048, 2017.

[20] N. Yamachi, T. Nishikawa, N. Sakai, K. Sawa, and M. Murakami, “Levitation forces of bulk superconductors in varying fields,” Physica C: Superconductivity, Vol.392-396, Part 1, pp. 579-584, 2003.

Name:
Tatsuya Nakasaki

Affiliation:
Faculty of Computer Science and Systems Engineering, Kyushu Institute of Technology

Address:
680-4 Kawazu, Iizuka, Fukuoka 820-8502, Japan

Brief Biographical History:

2019- Graduate School of Computer Science and Systems Engineering, Kyushu Institute of Technology

Name:
Yushi Kinoshita

Affiliation:
Faculty of Computer Science and Systems Engineering, Kyushu Institute of Technology

Address:
680-4 Kawazu, Iizuka, Fukuoka 820-8502, Japan

Brief Biographical History:
2019- Graduate School of Computer Science and Systems Engineering, Kyushu Institute of Technology

Name:
Panart Khajornrungruang

Affiliation:
Associate Professor, Department of Intelligent and Control Systems, Faculty of Computer Science and Systems Engineering, Kyushu Institute of Technology

Address:
680-4 Kawazu, Iizuka, Fukuoka 820-8502, Japan

Brief Biographical History:
2000 Graduated from Industrial Machinery Engineering, Osaka University
2005 Received Ph.D. from Department of Mechanical Engineering and Systems, Osaka University
2005- Research Associate, Advanced Mold and Die Technology Center, Kyushu Institute of Technology
2007- Assistant Professor, Kyushu Institute of Technology
2016- Associate Professor, Department of Mechanical Information Science and Technology, Faculty of Computer Science and Systems Engineering, Kyushu Institute of Technology
2019- Associate Professor, Department of Intelligent and Control Systems, Faculty of Computer Science and Systems Engineering, Kyushu Institute of Technology

Main Works:
- Laser applied precision engineering
- Live 3D nanoparticles observation
- R&D for CMP process technology

Membership in Academic Societies:
- Japan Society for Precision Engineering (JSPE)
- Japan Society of Mechanical Engineers (JSME)
- Japan Society for Abrasive Technology (JSAT)

Name:
Edmund Soji Otabe

Affiliation:
Professor, Department of Physics and Information Technology, Faculty of Computer Science and Systems Engineering, Kyushu Institute of Technology

Address:
680-4 Kawazu, Iizuka, Fukuoka 820-8502, Japan

Brief Biographical History:
1987 Graduated from Kyushu University
1991- Research Associate, Kyushu Institute of Technology
1997 Received Ph.D. from Kyushu University
2008- Professor, Department of Computer Science and Electronics, Faculty of Computer Science and Systems Engineering, Kyushu Institute of Technology
2019- Professor, Department of Physics and Information Technology, Faculty of Computer Science and Systems Engineering, Kyushu Institute of Technology

Main Works:
- Application of using superconducting materials
- "Fabrication of 1 T Bi-2223 superconducting magnet with 92 mm bore diameter at 77 K," Advances in Cryogenic Engineering, Vol.1573, pp. 754-759, 2014.

Membership in Academic Societies:
- Cryogenic and Super conductivity Society of Japan (CSSJ)
- Japan Society of Applied Physics (JSAP)
- Institute of Electronics, Information and Communication Engineers (IEICE)

Name:
Keisuke Suzuki

Affiliation:
Professor, Department of Intelligent and Control Systems, Faculty of Computer Science and Systems Engineering, Kyushu Institute of Technology

Address:
680-4 Kawazu, Iizuka, Fukuoka 820-8502, Japan

Brief Biographical History:
1993 Graduated from Nagoya Institute of Technology
1998 Received Ph.D. from Japan Advanced Institute of Science and Technology
2016- Professor, Department of Mechanical Information Science and Technology, Faculty of Computer Science and Systems Engineering, Kyushu Institute of Technology
2019- Professor, Department of Intelligent and Control Systems, Faculty of Computer Science and Systems Engineering, Kyushu Institute of Technology

Main Works:
- Chemical mechanical polishing
- Development semiconductor process
- R&D for nano materials
- Advanced processing technology

Membership in Academic Societies:
- Japan Society for Precision Engineering (JSPE)
- Japan Society of Applied Physics (JSAP)
- Japan Society of Mechanical Engineers (JSME)